© 2016. Published by The Company of Biologists Ltd | Journal of Cell Science (2016) 129, 2064-2074 doi:10.1242/jcs.183244

RESEARCH ARTICLE

Two classes of short intraflagellar transport train with different 3D structures are present in *Chlamydomonas* flagella

Elisa Vannuccini[1], Eugenio Paccagnini[1], Francesca Cantele[2], Mariangela Gentile[1], Daniele Dini[1], Federica Fino[1], Dennis Diener[3], Caterina Mencarelli[1] and Pietro Lupetti[1,*]

ABSTRACT

Intraflagellar transport (IFT) is responsible for the bidirectional trafficking of molecular components required for the elongation and maintenance of eukaryotic cilia and flagella. Cargo is transported by IFT 'trains', linear rows of multiprotein particles moved by molecular motors along the axonemal doublets. We have previously described two structurally distinct categories of 'long' and 'short' trains. Here, we analyse the relative number of these trains throughout flagellar regeneration and show that long trains are most abundant at the beginning of flagellar growth whereas short trains gradually increase in number as flagella elongate. These observations are incompatible with the previous hypothesis that short trains are derived solely from the reorganization of long trains at the flagellar tip. We demonstrate with electron tomography the existence of two distinct ultrastructural organizations for the short trains, we name these 'narrow' and 'wide', and provide the first 3D model of the narrow short trains. These trains are characterized by tri-lobed units, which repeat longitudinally every 16 nm and contact protofilament 7 of the B-tubule. Functional implications of the new structural evidence are discussed.

KEY WORDS: Intraflagellar transport, *Chlamydomonas* flagella, Flagellar regeneration, Electron tomography

INTRODUCTION

Cilia and flagella are highly specialized hair-like organelles exposed at the surface of eukaryotic cells, where they play sensory and motility functions crucial for cell physiology. Defects in the structure and/or the signalling function of either motile cilia or the primary cilium – a single cilium occurring on a wide variety of somatic cells – lead to developmental defects and to pathological conditions collectively referred to as ciliopathies (Badano and Katsanis, 2006; Fry et al., 2014; Madhivanan and Aguilar, 2014).

Cilia and flagella are dynamic structures whose assembly and disassembly are coupled with the cell cycle (reviewed by Pan et al., 2013). Once formed, they undergo a continuous turnover at their distal tip, where new components are added and turnover products are removed (Johnson and Rosenbaum, 1992; Rosenbaum and Child, 1967). Hence, precursors must be continuously supplied to the ciliary or flagellar compartment from the cell body, where they are synthesized. Such a selective transport depends on intracellular transport machineries and, particularly, on intraflagellar transport (IFT), a bidirectional motility process occurring in the space between axonemal microtubules and the flagellar membrane. IFT was first observed with differential interference contrast (DIC) microscopy in *Chlamydomonas* flagella (Kozminski et al., 1993). Most proteins of the IFT system have been characterized, and the general features of the IFT machinery have been remarkably conserved during evolution (Avidor-Reiss et al., 2004; Cole, 2003; Follit et al., 2009; Li et al., 2004; Pazour et al., 2000). Central to the IFT process are large multiprotein complexes, the IFT particles, which act as platforms for transport of cargoes, including axonemal and membrane proteins, signal transduction components and turnover products (Bhogaraju et al., 2013; Craft et al., 2015; Hao et al., 2011; Hou et al., 2007; Huang et al., 2007; Ishikawa et al., 2014; Mukhopadhyay et al., 2010; Qin et al., 2004, 2005; Viswanadha et al., 2014; Wren et al., 2013). Heterotrimeric kinesin II moves IFT particles from the ciliary base to the tip, whereas the cilium-specific cytoplasmic dynein 1b returns them from tip to base (Kozminski et al., 1995; Pazour et al., 1998, 1999; Porter et al., 1999); homodimeric kinesin OSM-3 cooperates with kinesin II in the assembly of *Caenorhabditis* sensory cilia (Snow et al., 2004). The IFT system interacts with the BBSome, a complex formed by proteins whose dysfunction is involved in the human ciliopathy Bardet-Biedl syndrome. The BBSome is moved along the axoneme by IFT and is involved in multiple functions, such as protein trafficking to the ciliary membrane, control of protein entry into cilia (Berbari et al., 2008; Loktev et al., 2008; Nachury et al., 2007; Seo et al., 2009; Su et al., 2014) and, in *Chlamydomonas*, exit of signalling proteins from the flagellar compartment (Lechtreck et al., 2009, 2013).

IFT particles comprise >20 polypeptides, arranged into the subcomplexes IFT-A and IFT-B (reviewed by Cole, 2003; Taschner et al., 2012). Although the direct interaction of the two subcomplexes *in vivo* is suggested by a series of evidence (Cole et al., 1998; Mencarelli et al., 2013; Ou et al., 2005; Qin et al., 2004; Rampolas et al., 2007; Silva et al., 2012; Wei et al., 2012), they are thought to play non-overlapping roles. In fact, mutations affecting IFT-A polypeptides are compatible with cilium assembly but result in a phenotype characterized by reduced retrograde transport and by the accumulation of IFT-B polypeptides at the ciliary tip (see for example Absalon et al., 2008; Deane et al., 2001; Follit et al., 2006; Pazour et al., 2000). Defects in most IFT-B polypeptides result instead in little or no ciliary assembly owing to the impairment of anterograde transport (Absalon et al., 2008; Iomini et al., 2001, 2009; Pazour et al., 1998; Tsao and Gorovsky, 2008). Thus, IFT-B and IFT-A have been respectively implied in anterograde and retrograde IFT motility.

Electron microscopy studies have shown that IFT particles multimerize *in vivo* and are moved along the axoneme as trains of particles (Kozminski et al., 1995). In the current model, IFT particles shuttle between a cytoplasmic pool and the ciliary

[1]Department of Life Sciences, University of Siena, Via Aldo Moro 2, 53100 Siena, Italy. [2]Dipartimento di Chimica, Università degli Studi di Milano, Via Camillo Golgi 19, 20133 Milan, Italy. [3]Department of Molecular, Cellular and Developmental Biology, Yale University, 219 Prospect Street, New Haven, CT 06520, USA.

*Author for correspondence (pietro.lupetti@unisi.it)

Received 16 November 2015; Accepted 30 March 2016

Journal of Cell Science

Journal of Cell Science (2016) 129, 2064-2074 doi:10.1242/jcs.183244

compartment, assemble into anterograde-moving trains at the base of the cilium and then move up to the ciliary tip, where they dissociate and unload their cargoes before being re-organized into retrograde-moving trains that move back to the ciliary base (Pedersen et al., 2006). In such a cyclic system, important regulatory events must take place at the ciliary base to monitor the assembly of trains and regulate their entry into flagellar compartment and at the tip, for cargo unloading, the conversion of anterograde-moving trains into those that move in a retrograde manner and the uploading of recycling products. These regulatory events are expected to be crucial not only for ciliary assembly but also for ciliary length control; however, molecular information on these processes is still largely missing.

Besides the high-resolution structures recently produced for small IFT subcomplexes (Bhogaraju et al., 2011; Taschner et al., 2011; Taschner et al., 2014), the ultrastructural organization of the IFT system has been so far only partially investigated. By using transmission electron microscopy (TEM), observations on *Chlamydomonas* flagella (Kozminski et al., 1995; Pedersen et al., 2006; Pigino et al., 2009) have identified IFT complexes as linear trains of electron-dense particles (Kozminski et al., 1995; Pedersen et al., 2006). Two different categories of trains have been detected in *Chlamydomonas* flagella, each one characterized by a distinct ultrastructure: 'short' trains, with a thicker, more electron-opaque aspect, a 16-nm repeat and a mean length of ∼250 nm; and 'long' trains, showing a less compact, more electron-transparent appearance, a 40-nm repeat and a mean length of ∼700 nm (Pigino et al., 2009). On the basis of their different morphologies, the two classes of trains have been suggested to play different functions.

Long IFT trains have proved to be more amenable for three-dimensional (3D) modelling using electron tomography than short trains. We performed a detailed ultrastructural analysis of *in situ* long trains, providing a model that confirms the regular repeat of particles within the train, and the occurrence of links between particles as well as to both the flagellar membrane and the B-tubule (Pigino et al., 2009). The short IFT trains appear, instead, to be more compact and elusive to the available strategies for 3D modelling.

Information on the organization of long trains has been obtained in the *fla14* mutant, where the function of the retrograde motor dynein 1b is impaired but anterograde transport is normal (Pazour et al., 1998). Because long trains are the only category of IFT trains detected in *fla14* cells, we have suggested previously that they are related to anterograde transport (Pigino et al., 2009), whereas the absence of short trains has been interpreted as being suggestive of their implication in the retrograde transport. Thus, both the structure and the function of short trains still lack a better definition.

With the aim to obtain further insights into the function of long and short IFT trains, we analysed their occurrence in both regenerating and resorbing flagella of *Chlamydomonas*.

Our results revealed an unexpected scenario, suggesting that short trains are used in full-length flagella for both anterograde and retrograde transport, being the only kind of trains identified in these flagella. By performing electron tomography, we also revealed the occurrence, in *Chlamydomonas* flagella, of two subtypes of short trains, each one with its own architecture. Once the presence of two distinct populations of short trains had been established, we could obtain, by an ad-hoc alignment and averaging strategy, the first tomographic reconstruction of the periodic structural unit of one of the two subtypes.

RESULTS

Monitoring long and short IFT trains during flagellar regeneration

We set out to measure the prevalence of long and short trains in growing flagella as a means to dissect their respective functions. Following deflagellation of *Chlamydomonas*, we observed kinetics of flagellar growth similar to that first described by Rosenbaum et al. (1969) (Fig. S1). From thin sections of flat-embedded cells processed at different regeneration times, we collected more than 1000 TEM micrographs; we analysed only flagellar longitudinal sections that included the central pair complex, which provide optimal lateral views of the trains. Because it is not possible to recover an entire longitudinal central section from a single flagellum (see Materials and Methods), in order to calculate the number of trains per flagellum at each regeneration time, first we measured and summed up the lengths of all the detected portions of flagellar central sections; this value was then divided by the average flagellar length observed at each regeneration time to generate the number of observed flagella. Table S1 shows the crude data obtained for each regeneration time – i.e. the number of counted trains and the combined lengths of flagellar sections inspected (in μm).

The length of both long and short IFT trains is maintained during regeneration

At any regeneration time, we could detect both short and long IFT trains (Fig. 1). The two types of trains can be distinguished on the basis of their length (∼300 nm and ∼700 nm, respectively) and periodicity (16 nm and 40 nm, respectively). Long trains are spread-out structures characterized by a wave pattern, visible in longitudinal sections (Fig. 1A) (Pigino et al., 2009). In contrast, short trains appear as more compact electron-opaque structures, in which particles appear sometimes to form a longitudinal rod-like element (Fig. 1B). The structural diversity between short and long trains allows unequivocal characterization of each train observed during flagellar regeneration. The discrepancy between the average length of short trains established in the present study and that reported previously (250 nm, Pigino et al., 2009) is probably due to the fact that the slender extension occurring at one end of one of the two subtypes of short trains (see below) was not carefully included in the measurements performed in that study.

The length and structure of the short and the long IFT trains were constant during flagellar regeneration (Fig. 1A–C), indicating that the length of both train types is tightly regulated. This is particularly evident for short trains, the length of which is quite strictly conserved during regeneration, as can be easily seen in Fig. 1B. The average length of long trains varied relatively little throughout regeneration, although it exhibited a higher standard deviation, likely owing to the greater difficulty in capturing the whole length of a long train within a single section.

Long and short IFT trains show inverse quantitative trends during flagellar regeneration

We analysed quantitatively the presence of long and short trains during regeneration. On the basis of the raw data reported in Table S1, and following the procedure described in the Materials and Methods, we calculated the content per flagellum in each class of train at each regeneration time. Unlike train length, the number of trains varied significantly throughout regeneration, with long and short trains showing inverse trends (Fig. 1D). Long trains were most abundant early during regeneration (15 min), decreased rapidly to about one third of their original amount at 30 min and then remain almost constant in number until the flagella were full

Journal of Cell Science (2016) 129, 2064-2074 doi:10.1242/jcs.183244

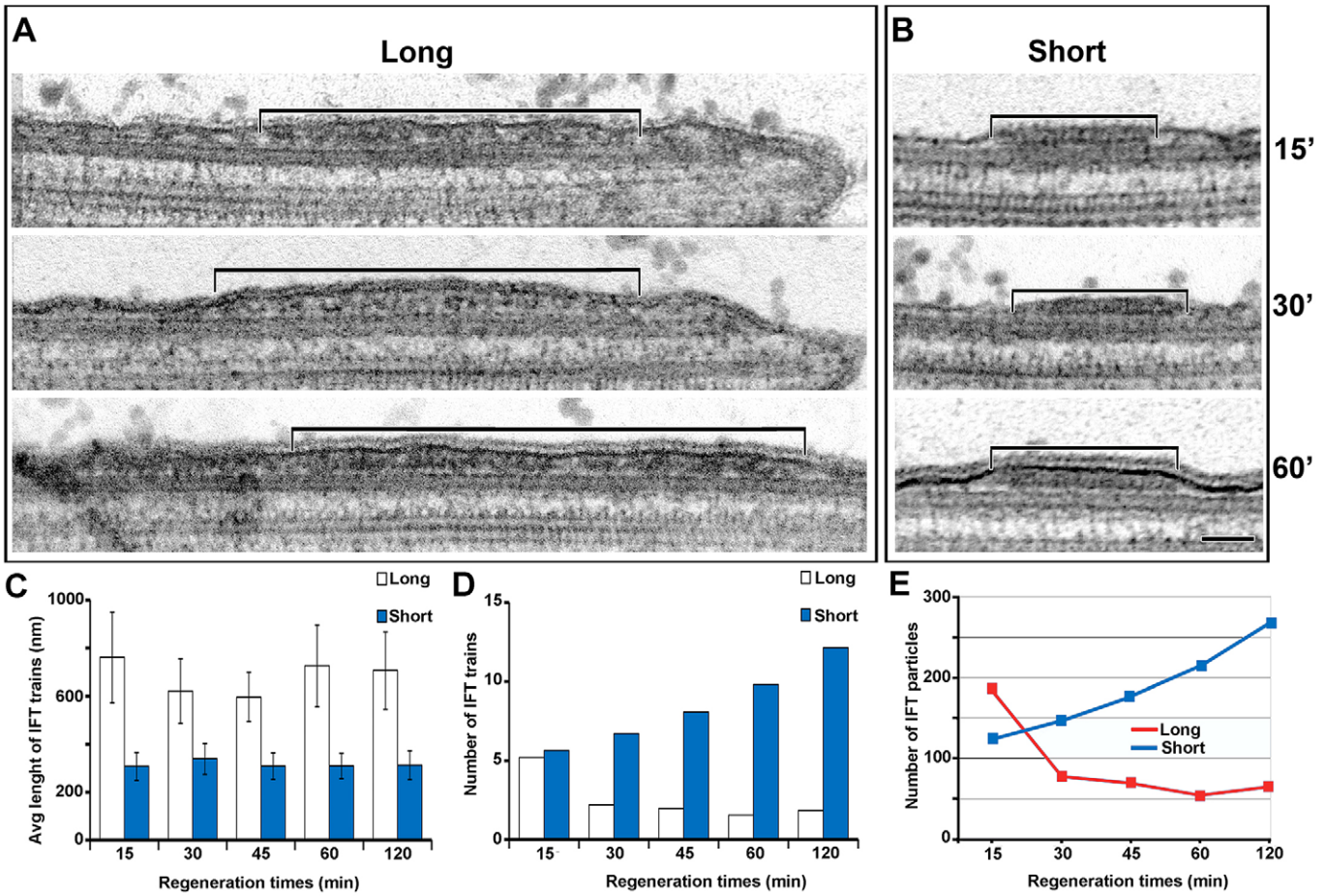

Fig. 1. Long and short IFT trains maintain their ultrastructure and length, but the relative abundance of the structures varies during flagellar regeneration. Transmission electron micrographs of flagella. (A) Long and (B) short trains are indicated. A rod-like element is sometimes visible in the short trains (e.g. the short train shown here for 15 min regeneration time). Scale bar: 100 nm. The histograms show, at different regeneration times, (C) the average length of long and short IFT trains (data are from ~500 µm of longitudinal flagellar sections inspected at each regeneration time; see Table S1), (D) the number of long and short trains per flagellum and (E) the number of IFT particles per flagellum that are expected to be involved in the assembly of long and of short trains. The amounts of particles forming the two classes of IFT trains are balanced at ~22 min.

length. The number of short trains, in contrast, was roughly equal to that of long trains at 15 min, but increased constantly during regeneration, reaching ~sevenfold the number of long trains in full-length flagella. Thus, the relative amount of the two classes of trains varies during regeneration, with long trains being the predominant class of IFT trains in short flagella, and short trains becoming highly predominant over long trains in full-length flagella.

The amount of particles forming long trains balances that of short trains in half-length flagella

According to the 3D model proposed by Pigino et al. (2009), long trains are formed by two parallel series of particles, containing two particles every 40 nm. In this model, the volume of each repeat is estimated to be about 10,000 nm^3, that is, a single particle occupies a volume of about 5000 nm^3.

Our electron tomographic analysis on short trains (see below) provided 3D models containing a volume of about 5000 nm^3 for each 16-nm repeat; this value was found to be about the same for both subtypes of short train (see below). Thus, each repeat of short trains contains about half the mass volume of each repeat of the long trains. We thus assumed that short and long trains contain one and two particles per longitudinal repeat, respectively.

Given the average train lengths reported in Fig. 1C, a long train appears to contain ~35 particles, which is almost twice the 18 particles expected to be contained in a short train. We roughly estimated the total amount of particles contained in each class of trains at each regeneration time, per flagellum (Fig. 1E). At 15 min, long trains equal short trains in number, but the amount of particles forming long trains was roughly twice the number of particles forming short trains; this ratio was balanced at a regeneration time of ~22 min – i.e. when flagella are ~6 µm long – and was inverted from 30 min of regeneration onward, when particles are predominantly assembled into short trains.

Short IFT trains display two different architectures

The above reported data show that, as flagella approach their full length, short trains become more abundant than long trains. Because anterograde transport must be balanced by retrograde transport – indeed we did not observe any accumulation of IFT-like material at flagellar tip at any regeneration time – these findings are in contrast with our previous hypothesis that long trains are the only anterograde-moving trains (Pigino et al., 2009) and suggest that short trains also contribute to anterograde transport. This in turn implies that short trains are bidirectional, comprising both anterograde- and retrograde-moving components.

Journal of Cell Science (2016) 129, 2064-2074 doi:10.1242/jcs.183244

We therefore decided to focus on short trains in order to (i) establish whether they represent a homogeneous population or, instead, they comprise structurally, and hence possibly functionally, distinct subpopulations of trains, and (ii) provide new insights into their ultrastructure.

While reviewing our electron micrographs of IFT trains *in situ*, we noticed that a subset of short trains was characterized by a polarized architecture, with a thin, slender contour at one end and a rounded contour at the opposite extremity (Fig. 2B); such a polarity is less evident in other short trains, which appear to be flanked by electron-transparent spots at both ends (Fig. 2A). Interestingly, all the short trains we could observe showing an evident polarity were oriented with their tapered end towards the flagellar tip (Fig. 2B).

In order to obtain more detailed ultrastructural information, we undertook a tomographic analysis of short trains *in situ*. We collected 134 double-tilt axis tomograms from full-length flagella and selected for the successive processing (see below) 43 tomograms on the basis of (i) their optimal resolution and (ii) the occurrence of the whole train within the thickness of the section. Upon analysing the selected tomograms, we found that short trains could indeed be categorized into two structural subclasses (Fig. 2E–H). The first subclass (26 tomograms) comprised a group of short trains sharing a more compact organization, with a lateral extension only slightly wider than the underlying doublet (Fig. 2D). Because of this ultrastructural feature, from now on, we refer to such a configuration as ‘narrow’. The second subtype (17 tomograms) was characterized by a looser organization, with a flattened structure and a lateral extension over the doublet about twofold wider than that of the narrow type (Fig. 2C); we named such trains ‘wide’. The reduced lateral width of narrow short trains with respect to wide trains is clearly visible in top longitudinal views of raw tomograms, where IFT trains are seen from the outside of the axoneme to be sitting on top of doublets (Fig. 2G,H); such views also confirmed that the two types of short train have similar, although not identical, lengths. Interestingly, the narrow configuration was characterized by the occurrence of a thin end projection, pointing towards the tip of the axoneme and located offset to the central longitudinal axis of the train (Fig. 2H). As a whole, narrow short trains are characterized by a polarized and laterally asymmetrical organization along their longitudinal axis. In contrast, no thin projection was visible at either end of wide short trains. Thus, the occurrence of two distinct ultrastructural subtypes of short trains was confirmed by the tomographic data.

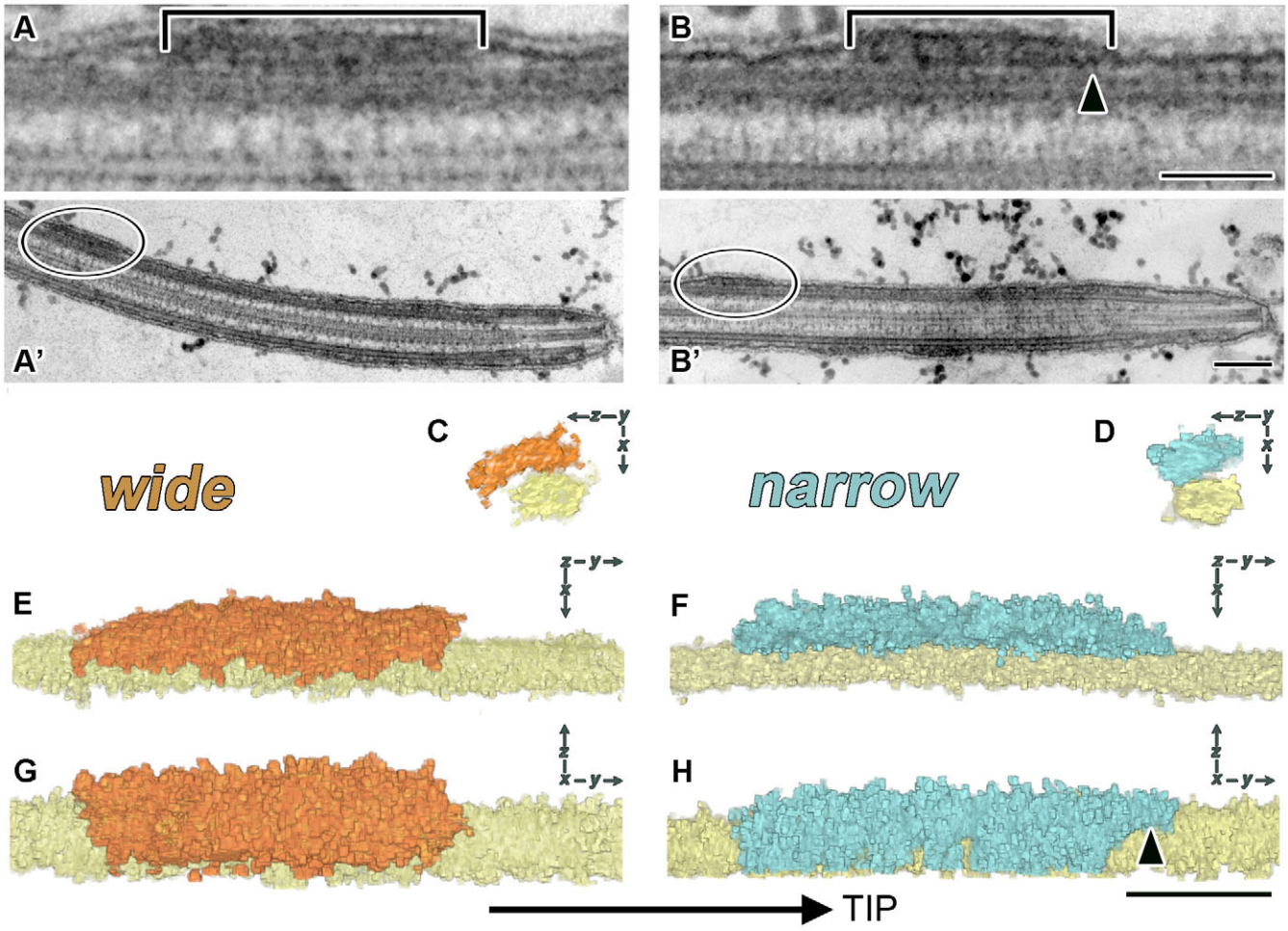

Fig. 2. Subtypes of short IFT trains. (A,B) The two subtypes of short trains can be distinguished in TEM images by the absence (A) or the presence (B) of a slender projection pointing toward the flagellar tip. Circles in A′,B′ mark the position along flagella of the trains shown in A,B. Scale bars: 100 nm (in B for A,B); 200 nm (in B′ for A′,B′). (C–H) Raw tomograms of the wide (orange) and narrow (pale blue) short IFT trains. (C,D) Cross views, (E,F) side views, (G,H) top views. The wide short trains are characterized by a lateral extension over the underlying microtubular doublet (light yellow) that is about twofold wider than that of the narrow short trains. The thin projection of narrow trains is indicated by an arrowhead in panels B and H. Scale bar: 100 nm (in H for C–H).

Journal of Cell Science (2016) 129, 2064-2074 doi:10.1242/jcs.183244

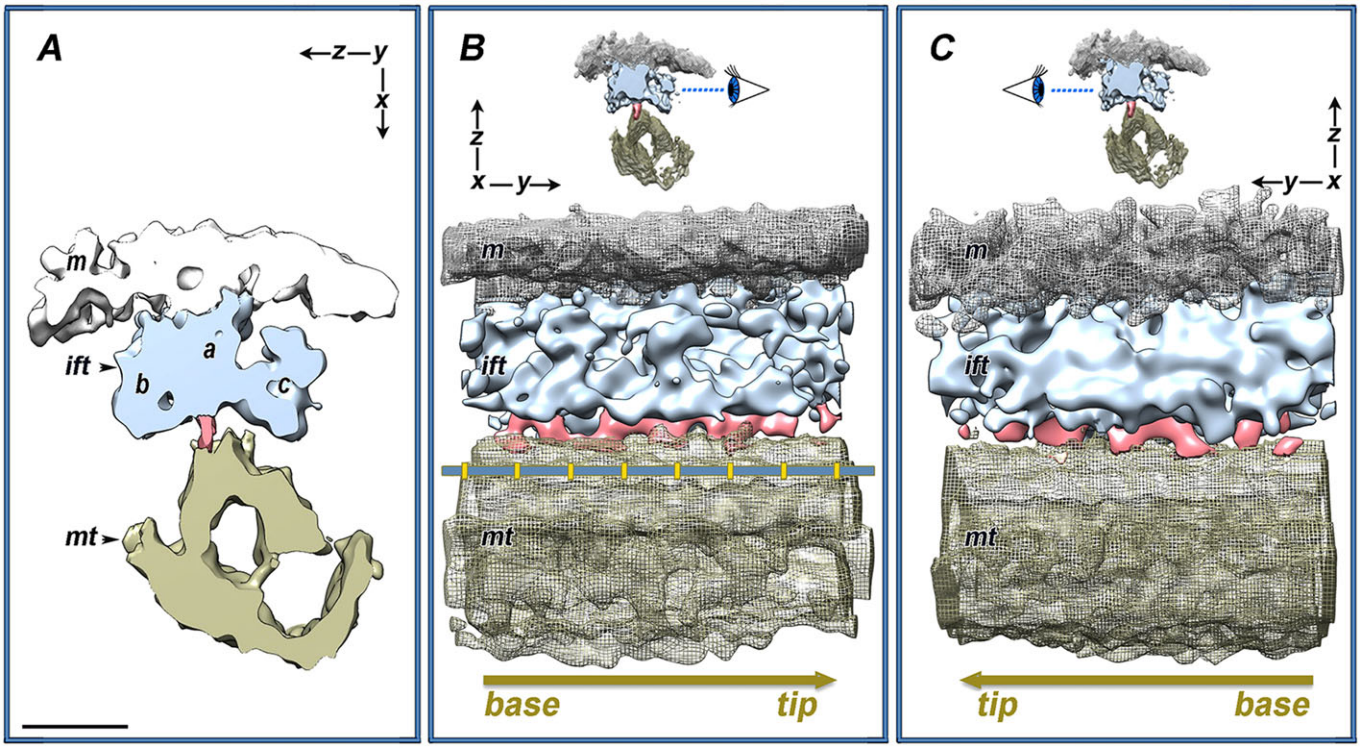

Fig. 3. Surface rendering of the segmented 3D model of the narrow short IFT trains. (A) Cross section of the model, viewed from the axoneme base. This section is shown as a reference in the upper part of B,C, where the small eyes indicate the vantage points used for visualization of the models below; arrows in both panels show the position of the flagellar base and tip. The yellow notches on the blue ruler in B have a pitch of 8 nm. m, membrane (white); ift, IFT train (pale blue); mt, microtubular doublets (beige). The links between the train and the microtubular surface are in pink. The organization of the train, with a central major domain, 'a', flanked by two lateral lobes, 'b' and 'c', is evident in A, along with its contact points with the membrane and the microtubule. Side views in B and C show the different structures of lateral lobes – the c lobe exhibits a periodicity of ∼16 nm and the b lobe is almost continuous. Scale bar: 16 nm (in A for A–C).

3D modelling of short narrow IFT trains reveals new ultrastructural features

Raw tomograms of both subclasses of IFT trains were processed with the ad-hoc alignment and averaging strategy described in the Materials and Methods. The application of a customized sub-tomogram averaging protocol to a homogeneous class of trains allowed us to consistently increase the signal-to-noise ratio with respect to the previously reported tomographic data for short trains (Pigino et al., 2009). This approach, however, produced a 3D model for the narrow short trains only, while so far, we have been unable to obtain an informative model for the wide short trains, probably owing to their looser and more fuzzy appearance, which made subtomogram alignment and averaging less effective. It is noteworthy that the averaged 3D model of the narrow short trains carries the structural features that are shared by all the trains whereas cargoes, because of their heterogeneity, are not expected to contribute significantly to the model.

Different views of the 3D model obtained for narrow short trains are shown in Figs 3–5; Movie 1 shows a rotating model. This model, comprising three repeating units, was obtained by focusing the alignment on the central unit and without imposing any symmetry. As a consequence, the three units are not identical, and the central one is the most reliable.

Cross sections of the segmented tomogram show the presence of a central major domain (a in Fig. 3A), bridging the inner aspects of flagellar membrane with the surface of the B-tubule. The central domain is flanked by two lobes (b and c in Fig. 3A) with different size and architecture. The b lobe – located on the left when viewing the train cross section from the base of the axoneme – is a compact structure tightly linked to the central domain. The c lobe, on the right side of the train, is instead separated from the central domain by a well-visible cleft (Fig. 4A).

Lateral views of the model confirm that the two lateral lobes possess distinct structural features. Lobe b appeared to be almost continuous (Fig. 3C), whereas the right lobe (c) exhibited a definite 16 nm periodicity (Fig. 3B). Such a periodicity results from the presence of repeating structural elements, each comprising a globular subdomain, a thinner stem and a basal subdomain that contacts the corresponding region of adjacent elements. Such an arrangement is reminiscent of the series of lollipop-like particles that have been previously visualized with transmission electron microscopy (e.g. figure 3 in Kozminski et al., 1995). The organization of each lollipop-like unit into three subdomains and the contacts among adjacent units through their basal subdomains are even more clearly appreciable in longitudinal sections (Fig. 5B, red frames).

Fig. 4 compares a cross section of the 3D model cut at the region intercalated between two adjacent lollipop-like units (Fig. 4A) with one section through the lollipop-like unit itself (Fig. 4C). The left lobe hosts cavities in either its upper or lower part, depending on the sectioning level (Fig. 4A,C). These cavities are regularly arranged along the train, as indicated by the observation of longitudinal sections of the 3D model, cut along a plane parallel to the flagellar membrane (Fig. 5C).

The arrangement of the two lateral lobes and the central domain confers a peculiar longitudinal organization to the narrow short trains, that is, the train appears to be divided into two parallel longitudinal regions, separated from each other by a deep cleft (Fig. 5C). Domain a and b form together a compact rod, which is

Journal of Cell Science (2016) 129, 2064-2074 doi:10.1242/jcs.183244

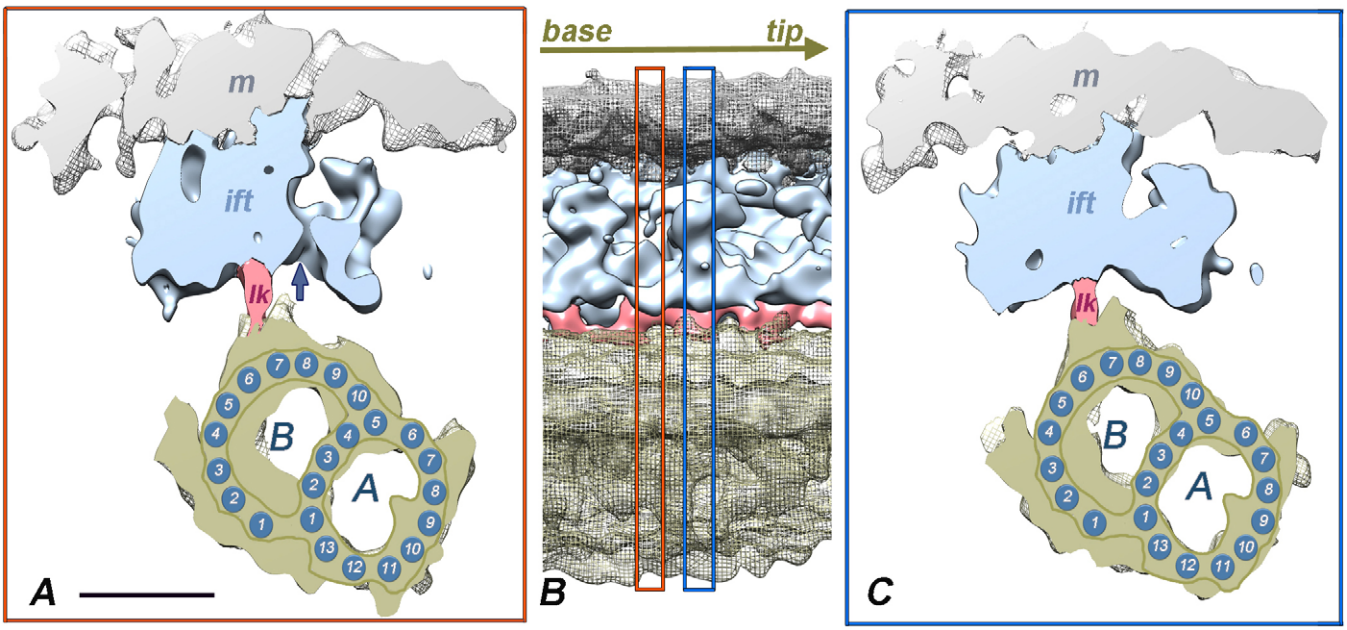

Fig. 4. Cross sections of the short narrow IFT train 3D model. (A) Cross section of the model, as shown in Fig. 3A, including protofilament numbering. 'A' and 'B' within the model denote the subtubules. The surface-rendering model in B shows the sectioning levels and the flagellum polarity. The blue arrow in A shows the space between the IFT particles framed in red in B. Such space is missing in frame C because the blue-framed section is centered on the IFT particle. The tubulin protofilament numbering from the established literature (blue numbered dots) was superimposed on cross sections of microtubule doublets, thereby allowing us to propose that the central row of links contacts the B-subtubule at its protofilament number 7. m, membrane; ift, intraflagellar transport train; lk, link. Scale bar: 16 nm (in A for A and C).

flanked on one side by a series of repeating longitudinal elements. We note that the tapered projection occurring at the extremity of the short narrow trains (Fig. 2H) is an extension of the compact longitudinal rod domain.

As noted above, the central domain establishes contacts with the membrane, on one side, and with the B-tubule surface, on the opposite side. The latter interaction was mediated by thin links (in pink in Figs 3–5). When a schematic representation of the doublet reporting the tubulin protofilament numbering was superimposed to a cross section of the reconstruction, the links appeared to contact the B-tubule at protofilament 7 (Fig. 4A,C). As evidenced in longitudinal sections of the reconstruction, the links are arranged in couples and contact the B-tubule surface with a periodicity of 8 nm (Fig. 5D).

Flagella from the conditional mutant *pf1fla10-1* reabsorb through an IFT-independent mechanism

In order to complete our observations, we also analysed the presence of IFT trains during flagellar resorption. We used the strain *pf1fla10-1*, a conditional double mutant that does not express a

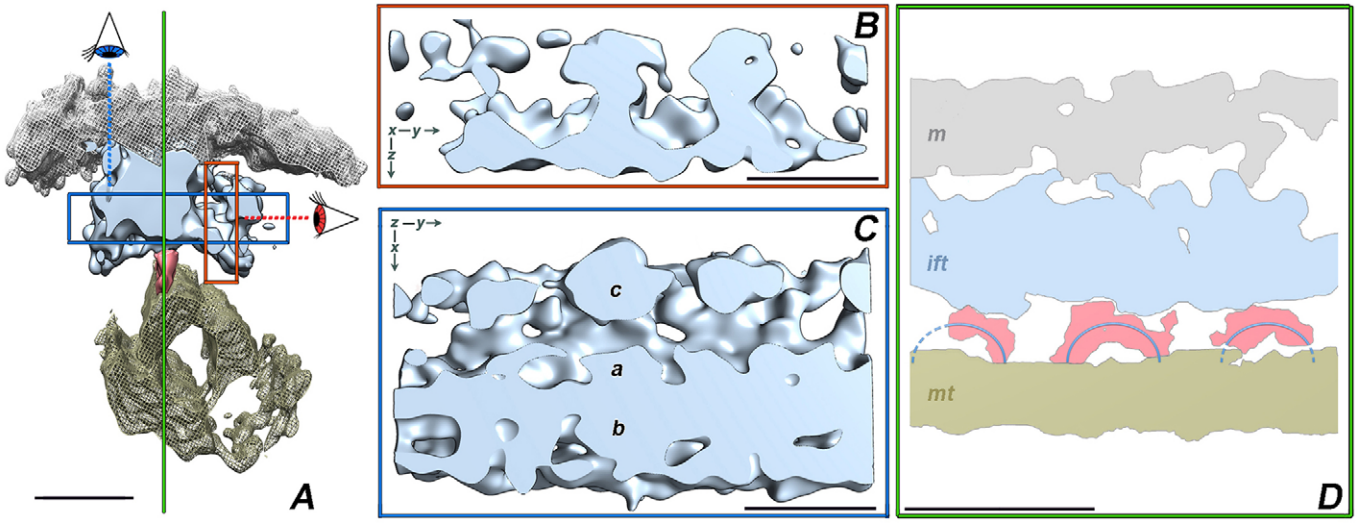

Fig. 5. Sagittal sections of the short narrow IFT train model. (A) Model of the narrow IFT train with the vantage points from which sections shown in B (red) and C (blue) are viewed. The green line shows the position of virtual sectioning along a single plane, shown in D. (B) Three interconnected bulges represent the IFT particles. (C) Removal of both the membrane and the top part of IFT model reveals the IFT periodic domains, 'c', and the continuous rod contributed by domains 'a' and 'b'. (C) Single-plane section cut through the connections between the links (pink) and the microtubule (mt). The light-blue arches indicate the links' geometry. m, membrane; ift, IFT train. Scale bars: 16 nm.

Journal of Cell Science (2016) 129, 2064-2074 doi:10.1242/jcs.183244

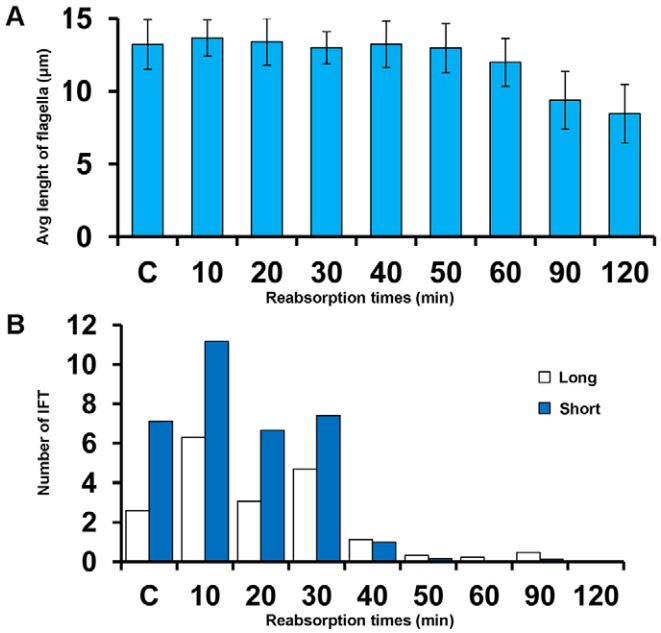

Fig. 6. Expression of IFT trains during flagellar shortening. (A) Average flagellar length; (B) number of long and short IFT trains at different resorption times (graphs were computed by using the data set shown in Table S2).

functional kinesin when incubated at 32°C. Flagellar shortening started after 60 min at 32°C (Fig. 6A). As in our analysis of flagellar regeneration, we collected TEM images for each resorption time and inspected them for the presence of long and short trains; from the data reported in Table S2, we computed the number of trains per flagellum (Fig. 6B).

pf1fla10-1 cells expressed a lower amount of flagellar IFT proteins than the wild-type strain (compare Figs 6B and 1D); this peculiarity has been described previously (Kozminski et al., 1995). The decrease in IFT content appeared to be mainly due to a decrease in the number of short trains with respect to what has been observed in wild-type flagella. Both long and short trains increased substantially over the first 10 min of exposure at the non-permissive temperature (Fig. 6B); however, this increase is transitory, and the number of both types of trains successively decreased and was maintained at approximately the original values until 40 min of incubation time, when an abrupt decrease to near-zero values was observed. Such behaviour is in good accordance with what has been previously demonstrated by Cole et al. (1998) by performing biochemical studies on the same mutant. These observations suggest that neither long nor short trains are involved in flagellar resorption and confirm that this process proceeds through an IFT-independent mechanism.

DISCUSSION

Short IFT trains are involved in anterograde transport

IFT particles continuously cycling between the cytoplasm and the flagellar compartment are first gathered in a pool at the flagellar base, where they associate with the basal body transitional fibres (Deane et al., 2001; Wei et al., 2013; Wood and Rosenbaum, 2014); from this pool, groups of particles organize into linear arrays – the IFT trains – and periodically enter the flagellum (Dentler, 2005; Ludington et al., 2013). The molecular mechanisms controlling the transit of particles through the transition zone and their organization into trains are largely unknown; similarly, very little is known about the molecular process controlling the reorganization of anterograde-moving trains into those moving in a retrograde manner at the tip, although, in *Chlamydomonas*, CDPK-1 has been recently implicated in kinesin-II inactivation and dissociation from the IFT-B subcomplex (Liang et al., 2014). At the end of their trip within the flagellar compartment, IFT particles return to the cytoplasm. Interestingly, although the flagellar compartment continuously exchanges IFT proteins with the cytoplasm, the amount of IFT protein per flagellum remains nearly constant throughout regeneration (Marshall and Rosenbaum, 2001; Marshall et al., 2005). Thus, reciprocal control of particles entering and exiting the flagellum results in a gradual reduction in IFT proteins per unit length in a growing flagellum and, possibly, a reduction of delivery of cargo to the tip. This observation was an important component of the initial 'balance-point model' of flagellar length control, in which length-dependent assembly is balanced against length-independent disassembly (Engel et al., 2009; Marshall et al., 2005; Marshall and Rosenbaum, 2001).

Until now, the available information has suggested that (i) only two categories of IFT trains exist, the long and the short trains, and that (ii) the anterograde phase is carried out by the long trains only; conversely, short trains have been proposed as being responsible for the retrograde phase (Pigino et al., 2009). A 3D model is available for long trains (Pigino et al., 2009), but details of the architecture of short trains had not been described.

First, we have shown that long and short trains maintain their own length and architecture throughout the entire regeneration process. This suggests that specific size and ultrastructure constraints act during the assembly of each type of train and that the function of each train is tied to its specific ultrastructure. Our second finding is that the relative abundance of long and short trains changes during regeneration: long trains predominate early in flagellar regeneration, whereas short trains are dominant in full-length flagella.

Based on total internal reflection fluorescence (TIRF) microscopy of flagella of strains expressing IFT–GFP fusion proteins, Engel et al. (2009) proposed that a length-dependent remodelling of train size underlies the decrease in anterograde transport of precursors to the tip as the flagellum approaches its full length. Using the intensity of the fluorescence signal as a measure of the number of GFP molecules within a single train, the authors estimated the relative size of anterograde trains at different regeneration times, and found them to be about twofold larger in short (2–6 µm) than in long (>8 µm) flagella, whereas very short flagella (<2 µm) were characterized by 3–4 times brighter trains. Interestingly, the same approach also revealed that anterograde trains are heterogeneous and comprise two populations of trains moving with different velocities – slower (~1.6 µm/s) in short regenerating flagella (<5 µm) and quicker (~2.3 µm/s) in flagella longer than 8 µm. Such heterogeneity has been confirmed by a study on *Trypanosoma* flagella (Buisson et al., 2013). In both organisms, the rate of retrograde transport appeared homogeneous (Buisson et al., 2013; Engel et al., 2012). Although TIRF microscopy does not provide any ultrastructural information or any direct evidence on the precise length of the imaged IFT trains, these observations suggest that short regenerating flagella possess anterograde trains that are larger and move more slowly than the anterograde trains present in longer flagella.

Our data on the differential presence of long and short trains during flagellar regeneration agree with the evidence quoted above, as well as with the results recently provided by Ludington et al. (2013). Those authors analysed the dynamics of IFT entry into the flagellum and showed that it occurs through periodic injections of

Journal of Cell Science (2016) 129, 2064-2074 doi:10.1242/jcs.183244

IFT proteins following an avalanche-like behaviour. The amount of IFT proteins entering the flagellum at a single injection event was found to be length-dependent – rapidly regenerating flagella have large infrequent injections, whereas full-length flagella are characterized by small and frequent injections. It seems plausible that the presence of long trains during the first regeneration phase corresponds to the injection of larger amounts of proteins, whereas the entry of smaller amounts of particles is related to the assembly and entry of short anterograde trains.

Our observation that the number of short trains increases linearly with regeneration time, whereas the number of long trains decreases, conflicts with our original hypothesis that short trains only move in the retrograde direction. If long trains move to the tip and reorganize to form the short trains that return to the cell body, the number of long and short trains should decrease in parallel during flagellar growth. Furthermore, for the previous model to be correct, the mass of long trains moving toward the tip should always equal the mass of short trains moving toward the cell body. These predictions are contradicted by the current measurements, so the previous model cannot be correct.

Because the amounts of long and short trains are clearly not balanced, our data indicate that short trains are involved in anterograde transport too. We thus propose that the anterograde motility is sustained by morphologically distinct types of trains, appearing at different times during flagellar regeneration, with the long trains being most abundant over the first half-time of regeneration, and the short trains being predominant in half- to full-length flagella.

The amount of IFT particles comprising the two populations of long and short trains is balanced in half-length flagella

Our computation of IFT-particle content in long and short trains per flagellum at each regeneration time showed that the two train types contain equivalent amounts of particles only at the regeneration time of ∼22 min, when the flagellum reaches a length of ∼6 µm, that is, about half-length. Although we do not know the specific function(s) of long and short trains, we think this finding is worth note. In fact, flagellar half-length seems to be a threshold length at which significant changes occur in the activity of kinases, like *Chlamydomonas* aurora-like kinase (CALK) (Pan et al., 2004; Luo et al., 2011) and GSK3β (Wilson and Lefebvre, 2004), which have been reported to play an essential role in flagellar assembly and disassembly. Interestingly, in vertebrate primary cilia, both Aurora A and GSK3 are part of signalling pathways involved in cilium maintenance (Dutta-Simmons et al., 2009; Thoma et al., 2007). It seems likely that the switching to the prevalence of short over long trains occurring in half-length flagella is part of a series of related, although largely unknown, events taking place in this specific phase of regeneration.

The 3D structure of narrow short IFT trains

Our previous attempts to produce a 3D model of short trains *in situ* in *Chlamydomonas* flagella were hampered by their density and heterogeneity (Pigino et al., 2009). Here, the discovery that short trains comprise two distinct structural arrays allowed us to overcome some of these limitations and to obtain the first resolved model of the narrow subtype of short trains.

We identified in the model three different structural regions. Two of them, the a and b lobes in Fig. 3, are so closely apposed that they form almost a single domain. We note that, in a cross section, this part of the train appears particularly well suited to accommodate complexes with the size and shape of isolated IFT particles (Mencarelli et al., 2013); the occurrence of small internal cavities is also a structural feature shared with isolated particles. These considerations suggest that the backbone structure of narrow short trains might be formed by stacked particles that are linked through motors to the doublet. We do not have any evidence about which motor is engaged on the doublet in these trains, but note that the organization of the 16-nm-repeating structural units occurring on one side of the train (lobe c) is compatible with that of inactive dynein molecules, whose ultrastructure has been recently described (Torisawa et al., 2014). If our hypothesis is correct, it would imply that narrow short trains move in an anterograde fashion.

The occurrence of multiple contacts between narrow short trains and the flagellar membrane is a feature that has also been previously observed in long trains (Pigino et al., 2009); membrane proteins have been shown to move along the flagellum at a speed matching that of IFT (Huang et al., 2007). Our model is thus in agreement with the available information suggesting that IFT complexes tend to keep an association with membrane while performing their functions.

Our model refers to the organization of the main region of the narrow short train. Raw tomograms also documented the presence of a pointed end-domain tapered onto the microtubule. We do not have any information about its fine structure and molecular composition. Finally, it is of note that the narrow short trains – as the previously described long trains – interact with the B-tubule. This observation indicates the existence of a specific motility pathway for IFT. The B-tubule is characterized by a content of post-translationally modified tubulin higher than the A-tubule and, in *Chlamydomonas*, glutamylated tubulin is preferentially localized in the B-tubule (Kubo et al., 2010). A regulatory role for tubulin post-translational modifications has been demonstrated for the interaction between motors and microtubules (Kubo et al., 2010, 2012; Suryavanshi et al., 2010), and might be expected to act on IFT motors as well.

Final considerations

Our data reveal an unexpected complexity in the ultrastructure of IFT trains. The three different architectural types we have identified are suggestive of different functions, although presently we have no information concerning the specific function of each train type or the directionality of the two types of short train.

The abundance of long trains at the onset of regeneration suggests that they play an important role at that time. These trains comprise a double parallel series of particles (Pigino et al., 2009) and are thus expected to contain a higher number of sites available for cargo binding and transport than might be thought for either narrow or wide short trains. Long trains could be devoted specifically to the transport of axonemal precursors, which are maximally required during the initial rapid growth exhibited by short regenerating flagella. The subsequent transition to a slow elongation phase as flagella approach their steady-state length (Rosenbaum et al., 1969) is coherent with the observed decrease in the number of long trains. In full-length flagella, fewer precursors are required to sustain axonemal turnover, and the small number of long trains present in these flagella could be sufficient to move them to the flagellar tip.

As to short trains, their delayed assembly would suggest that their function is characteristic of the late phase of flagellar assembly, and is maximally required in full-length flagella. They might be involved in functions like signal transduction, or be part of a still not completely defined signalling system that has been proposed to monitor flagellar length (Cao et al., 2013; Hilton et al., 2013).

From this perspective, it is interesting to recall here some information recently published on the role of the BBSome in *Chlamydomonas*. This complex is required for exit from the

Journal of Cell Science (2016) 129, 2064-2074 doi:10.1242/jcs.183244

flagellar compartment of some putative signalling proteins – e.g. phospholipase D (Lechtreck et al., 2013); at the same time, loss of the complex does not cause a general failure of the ciliary assembly machinery because flagella of mutants that are null for BBS proteins maintain their typical length (Lechtreck et al., 2009). On this basis, it has been proposed that a BBSome-specific function might be to transport signalling proteins. Interestingly, in *Chlamydomonas*, the BBSome is transported in both directions through IFT, but it does not associate with all IFT trains (Lechtreck et al., 2009).

In conclusion, our data suggest that in *Chlamydomonas* flagella, IFT is carried out by morphologically – and presumably functionally – distinct categories of IFT trains, the assembly of which appears to be under a strict temporal control during flagellar regeneration.

MATERIALS AND METHODS

Strains and culture conditions

Chlamydomonas reinhardtii wild-type strain 137c (provided by George Witman, University of Massachusetts, Worcester, MA) and the double-mutant strain *pf1fla10-1* (provided by Joel Rosenbaum, Yale University, New Haven, CT) were employed to monitor the presence of IFT trains during flagellar regeneration and resorption, respectively. *pf1fla10-1* is paralysed for a radial spoke defect (*pf1*) and carries a temperature-sensitive mutation (*fla10-1*) in the kinesin-II motor subunit FLA10 (Vashishtha et al., 1996; Walther et al., 1994) so that flagellar resorption can be induced by exposure to the non-permissive temperature of 32°C. Both strains were grown in Minimal Medium (MM) (Sager and Granick, 1953) at 23°C on 14 h–10 h light–dark cycle with constant aeration.

Transmission electron microscopy

137c cells were deflagellated by pH shock, as described previously by Lefebvre (1995). Samples of cells fixed at different regeneration times were split into two parts – one used to measure flagellar length by scanning electron microscopy (SEM) and the other processed for flat-embedding in Epon resin according to Geimer (2009). *pf1fla10-1* cells were exposed to the non-permissive temperature, fixed at incremental time points and flat-embedded.

Flat-embedded cells were cut with a Reichert Ultracut IIE ultramicrotome equipped with a Diatome Ultra 45° diamond knife; thin sections (60 nm) were collected on formvar-coated 75- or 100-square mesh copper grids, and stained with uranyl acetate and lead citrate (Reynolds, 1963). Samples were imaged by a FEI Tecnai G2 Spirit transmission electron microscope operating at an electron-accelerating voltage of 100 kV and fitted with an OSIS Morada CCD camera and ITEM software.

Electron tomography and 3D modelling

Thick sections (~160–180 nm) from flat-embedded flagella of wild-type cells were decorated on both faces with 10-nm colloidal gold particles before TEM analysis. Gold particles were used as position markers for image alignment during the tomogram reconstruction procedure. Tomography was performed with a Philips CM200 transmission electron microscope fitted with a field emission gun and at an electron-accelerating tension of 200 kV. For tomographic reconstruction, series of tilted images were recorded at low electron dose, in double-tilt axis geometry, at 27,500× magnification, with a maximum tilt range of about 60° and tilt steps of 1°. Tomograms were obtained from double-tilt data series by using the simultaneous alignment method (Cantele et al., 2010), which allows the reconstruction of all portions of the tomogram in every orientation by applying the proper positioning parameters directly to areas of the original 2D projections. After alignment, each tomogram was segmented using a semi-automatic method using Java User Segmentation Tool (JUST) (Salvi et al., 2008). The segmentation output consists of separate sets of voxels, each one representing one of the different structural arrays present in the tomogram. In the case of tomograms from flagellar portions containing IFT trains, segmentation allowed us to define the train, microtubular doublets, flagellar membrane and the surrounding glycocalyx, and to assign them to independent sets of voxels.

For preliminary alignment of trains from different subtomograms, we used a reference model of the doublet underlying each train, comprising two spline lines tracing the microtubule axes, together with the mass centre of the train. First, the line representing the B-tubule was set along the *z*-axis, with the axoneme tip pointing toward high values and the mass centre of the train lying on the *xy* plane; then, the model was rotated so that the segment passing from the centre of the B-tubule to that of the A-tubule could point toward the *x*-axis. The overall transformation was applied to the orientation parameters of the experimental projections, and the tomogram was reconstructed in that position. In this way, all trains were brought into the same position with respect to a unique coordinate system and could be averaged. The average was performed by merging directly 2D projections, not the 3D reconstructions of the single train, thus making it easier to compensate for missing regions by use of single-particle algorithms.

The IFT train average was refined by correlation alignment of 3D reconstructions. Owing to the structural variability intrinsic to IFT trains, which are not identical but quasi-equivalent structures, an optimized alignment strategy was used. First, some cycles of rigid alignment were performed. Then, each reconstruction was divided into small portions by Gaussian masks, and the resulting sub-regions were finally processed by local refinement. The rationale for the use of Gaussian masks is that each projection contributes with different parameters to different portions of the overall 3D average, thus limiting the individual contribution of each portion of 2D projections to the global average reconstruction. In addition, the use of Gaussian masks made it easier to evaluate the contribution of masks to the final reconstruction and to equalize it in the final model.

At the end of the alignment process, the resulting average model showed a defined periodicity; it was thus possible to identify repeating units that were further aligned and averaged to produce the final reconstruction of the train. The asymmetric ends of short trains were not included in the averaging because of their variability. The estimated resolution of our final model is 4–3.5 nm, based on the Fourier shell correlation (FSC) method (van Heel and Schatz, 2005). Such resolution is confirmed when using the ResMap software (Kucukelbir et al., 2014).

Length measurement of flagella and IFT trains *in situ*

For each regeneration (or resorption) time, the length of ~100 flagella was measured using SEM (not shown here), which provides a reliable imaging of the entire flagellum. TEM images from thin longitudinal sections of flat-embedded samples were used to measure the length of trains *in situ*. Because of the slight tilting of the sectioning plane with respect to the longitudinal flagellar axis, these sections show only flagellar portions, and it is impossible to visualize an entire flagellum in a single section. Only images of longitudinally sectioned flagella showing the central-pair microtubules were used to identify and measure trains *in situ*. All length measurements were performed on digital micrographs using ImageJ.

Computation of IFT train number per flagellum

In order to measure and classify trains *in situ*, we first calculated the number of trains observed per micron of the flagellar section. We then approximated the overall volume of a single flagellum to that of a cylinder with a 250-nm diameter and a length of 12 µm. The cross-section area of such a cylinder being 49,063 nm^2, we computed its volume to be ~0.589 μm^3. A 60-nm-thick longitudinal section comprising the whole central portion of a flagellum was then calculated to have a volume of ~0.178 μm^3, given that the area of the circular segment at its base is ~14,884 nm^2 and its length is ~12 µm. Thus, the volume of a flagellum sampled by a 60-nm-thick central section is about 30–34% of the entire flagellar volume. On this basis, the number of trains per flagellum was estimated by multiplying by 3296 the figures obtained by scoring the trains detected by TEM in the central axial sections of flagella.

Acknowledgements

Authors wish to thank Professor Joel L. Rosenbaum (Yale University) for having inspired a good part of this work and for many constructive discussions during manuscript preparation. Dr David Mercati is acknowledged for technical support.

Competing interests
The authors declare no competing or financial interests.

Author contributions
E.V. performed the electron microscopy analysis of IFT trains and contributed to the initial writing of the manuscript. E.P. collected and aligned the tomographic series; F.C. made the image analyses for 3D modeling; M.G., D. Dini and F.F. contributed to EM data collection and analysis. D. Diener contributed to interpretation of data and collaborated with manuscript writing. P.L. conceived the experiments, P.L. and C.M. interpreted the data and wrote the manuscript.

Funding
This work was supported by Progetti di Ricerca di Interesse Nazionale (PRIN) [grant number 2209JNTZ4L to P.L.] and a contribution by ChiantiBanca to C.M. D. Diener was supported by National Institutes of Health Grant [grant number GM014642 to Joel Rosenbaum]. Deposited in PMC for release after 12 months.

Supplementary information
Supplementary information available online at
http://jcs.biologists.org/lookup/suppl/doi:10.1242/jcs.183244/-/DC1

References
Absalon, S., Blisnick, T., Kohl, L., Toutirais, G., Dore, G., Julkowska, D., Tavenet, A. and Bastin, P. (2008). Intraflagellar transport and functional analysis of genes required for flagellum formation in Trypanosomes. *Mol. Biol. Cell* **19**, 929-944.

Avidor-Reiss, T., Maer, A. M., Koundakjian, E., Polyanovsky, A., Keil, T., Subramaniam, S. and Zuker, C. S. (2004). Decoding cilia function: defining specialized genes required for compartmentalized cilia biogenesis. *Cell* **117**, 527-539.

Badano, J. L., Mitsuma, N., Beales, P. L. and Katsanis, N. (2006). The ciliopathies: an emerging class of human genetic disorders. *Annu. Rev. Genomics Hum. Genet.* **7**, 125-148.

Berbari, N. F., Lewis, J. S., Bishop, G. A., Askwith, C. C. and Mykytyn, K. (2008). Bardet-Biedl syndrome proteins are required for the localization of G protein-coupled receptors to primary cilia. *Proc. Natl. Acad. Sci. USA* **105**, 4242-4246.

Bhogaraju, S., Taschner, M., Morawetz, M., Basquin, C. and Lorentzen, E. (2011). Crystal structure of the intraflagellar transport complex 25/27. *EMBO J.* **30**, 1907-1918.

Bhogaraju, S., Cajanek, L., Fort, C., Blisnick, T., Weber, K., Taschner, M., Mizuno, N., Lamla, S., Bastin, P., Nigg, E. A. et al. (2013). Molecular basis of tubulin transport within the cilium by IFT74 and IFT81. *Science* **341**, 1009-1012.

Buisson, J., Chenouard, N., Lagache, T., Blisnick, T., Olivo-Marin, J.-C. and Bastin, P. (2013). Intraflagellar transport proteins cycle between the flagellum and its base. *J. Cell Sci.* **126**, 327-338.

Cantele, F., Paccagnini, E., Pigino, G., Lupetti, P. and Lanzavecchia, S. (2010). Simultaneous alignment of dual-axis tilt series. *J. Struct. Biol.* **169**, 192-199.

Cao, M., Meng, D., Wang, L., Bei, S., Snell, W. J. and Pan, J. (2013). Activation loop phosphorylation of a protein kinase is a molecular marker of organelle size that dynamically reports flagellar length. *Proc. Natl. Acad. Sci. USA* **110**, 12337-12342.

Cole, D. G. (2003). The Intraflagellar Transport machinery of *Chlamydomonas reinhardtii*. *Traffic* **4**, 435-442.

Cole, D. G., Diener, D. R., Himelblau, A. L., Beech, P. L., Fuster, C. J. and Rosenbaum, J. L. (1998). *Chlamydomonas* Kinesin-II–dependent Intraflagellar Transport (IFT): IFT particles contain proteins required for ciliary assembly in *Caenorhabditis elegans* sensory neurons. *J. Cell Biol.* **141**, 993-1008.

Craft, J. M., Harris, J. A., Hyman, S., Kner, P. and Lechtreck, K. F. (2015). Tubulin transport by IFT is upregulated during ciliary growth by a cilium-autonomous mechanism. *J. Cell Biol.* **208**, 223-237.

Deane, J. A., Cole, D. G., Seeley, E. S., Diener, D. R. and Rosenbaum, J. L. (2001). Localization of intraflagellar transport protein IFT52 identifies basal body transitional fibers as the docking site for IFT particles. *Curr. Biol.* **11**, 1586-1590.

Dentler, W. (2005). Intraflagellar transport (IFT) during assembly and disassembly of *Chlamydomonas* flagella. *J. Cell Biol.* **170**, 649-659.

Dutta-Simmons, J., Zhang, Y., Gourgun, G., Gatt, M., Mani, M., Hideshima, T., Takada, K., Carlson, N. E., Carrasco, D. E., Tai, Y.-T. et al. (2009). Aurora kinase A is a target of Wnt/beta-catenin involved in multiple myeloma disease progression. *Blood* **114**, 2699-2708.

Engel, B. D., Ludington, W. B. and Marshall, W. F. (2009). Intraflagellar transport particle size scales inversely with flagellar length: revisiting the balance-point length control model. *J. Cell Biol.* **187**, 81-89.

Engel, B. D., Ishikawa, H., Wemmer, K. A., Geimer, S., Wakabayashi, K.-i., Hirono, M., Craige, B., Pazour, G. J., Witman, G. B., Kamiya, R. et al. (2012). The role of retrograde intraflagellar transport in flagellar assembly, maintenance, and function. *J. Cell Biol.* **199**, 151-167.

Follit, J. A., Tuft, R. A., Fogarty, K. E. and Pazour, G. J. (2006). The Intraflagellar Transport protein IFT20 is associated with the Golgi complex and is required for cilia assembly. *Mol. Biol. Cell* **17**, 3781-3792.

Follit, J. A., Xu, F., Keady, B. T. and Pazour, G. J. (2009). Characterization of mouse IFT complex B. *Cell. Motil. Cytoskeleton* **66**, 457-468.

Fry, A. M., Leaper, M. J. and Bayliss, R. (2014). The primary cilium: guardian of organ development and homeostasis. *Organogenesis* **10**, 62-68.

Geimer, S. (2009). Immunogold labeling of flagellar components in situ. *Methods Cell Biol.* **91**, 63-80.

Hao, L., Efimenko, E., Swoboda, P. and Scholey, J. M. (2011). The retrograde IFT machinery of C. elegans cilia: two IFT dynein complexes? *PLoS ONE* **6**, e20995.

Hilton, L. K., Gunawardane, K., Kim, J. W., Schwarz, M. C. and Quarmby, L. M. (2013). The kinases LF4 and CNK2 control ciliary length by feedback regulation of assembly and disassembly rates. *Curr. Biol.* **23**, 2208-2214.

Hou, Y., Qin, H., Follit, J. A., Pazour, G. J., Rosenbaum, J. L. and Witman, G. B. (2007). Functional analysis of an individual IFT protein: IFT46 is required for transport of outer dynein arms into flagella. *J. Cell Biol.* **176**, 653-665.

Huang, K., Diener, D. R., Mitchell, A., Pazour, G. J., Witman, G. B. and Rosenbaum, J. L. (2007). Function and dynamics of PKD2 in Chlamydomonas reinhardtii flagella. *J. Cell Biol.* **179**, 509-514.

Iomini, C., Babaev-Khaimov, V., Sassaroli, M. and Piperno, G. (2001). Protein particles in *Chlamydomonas* flagella undergo a transport cycle consisting of four phases. *J. Cell Biol.* **153**, 13-24.

Iomini, C., Li, L., Esparza, J. M. and Dutcher, S. K. (2009). Retrograde intraflagellar transport mutants identify complex A proteins with multiple genetic interactions in Chlamydomonas reinhardtii. *Genetics* **183**, 885-896.

Ishikawa, H., Ide, T., Yagi, T., Jiang, X., Hirono, M., Sasaki, H., Yanagisawa, H., Wemmer, K. A., Stainier, D. Y., Qin, H. et al. (2014). TTC26/DYF13 is an intraflagellar transport protein required for transport of motility-related proteins into flagella. *eLife* **1**, e01566.

Johnson, K. A. and Rosenbaum, J. L. (1992). Polarity of flagellar assembly in *Chlamydomonas*. *J. Cell Biol.* **119**, 1605-1611.

Kozminski, K. G., Johnson, K. A., Forscher, P. and Rosenbaum, J. L. (1993). A motility in the eukaryotic flagellum unrelated to flagellar beating. *Cell Biol.* **90**, 5519-5523.

Kozminski, K. G., Beech, P. L. and Rosenbaum, J. R. (1995). The *Chlamydomonas* kinesin-like protein FLA10 is involved in motility associated with the flagellar membrane. *J. Cell Biol.* **131**, 1517-1527.

Kubo, T., Yanagisawa, H.-a., Yagi, T., Hirono, M. and Kamiya, R. (2010). Tubulin polyglutamylation regulates axonemal motility by modulating activities of inner-arm dyneins. *Curr. Biol.* **20**, 441-445.

Kubo, T., Yagi, T. and Kamiya, R. (2012). Tubulin polyglutamylation regulates flagellar motility by controlling a specific inner-arm dynein that interacts with the dynein regulatory complex. *Cytoskeleton* **69**, 1059-1068.

Kucukelbir, A., Sigworth, F. J. and Tagare, H. D. (2014). Quantifying the local resolution of cryo-EM density maps. *Nat. Methods* **11**, 63-65.

Lechtreck, K.-F., Johnson, E. C., Sakai, T., Cochran, D., Ballif, B. A., Rush, J., Pazour, G. J., Ikebe, M. and Witman, G. B. (2009). The *Chlamydomonas reinhardtii* BBSome is an IFT cargo required for export of specific signaling proteins from flagella. *J. Cell Biol.* **187**, 1117-1132.

Lechtreck, K. F., Brown, J. M., Sampaio, J. L., Craft, J. M., Shevchenko, A., Evans, J. E. and Witman, G. B. (2013). Cycling of the signaling protein phospholipase D through cilia requires the BBSome only for the export phase. *J. Cell Biol.* **201**, 249-261.

Lefebvre, P. A. (1995). Flagellar amputation and regeneration in Chlamydomonas. *Methods Cell Biol.* **47**, 3-7.

Li, B. J., Gerdes, J. M., Haycraft, C. J., Fan, Y., Teslovich, T. M., May-Simera, H., Li, H., Blacque, O. E., Li, L., Leitch, C. C. et al. (2004). Comparative genomics identifies a flagellar and basal body proteome that includes the BBS5 human disease gene. *Cell* **117**, 541-552.

Liang, Y., Pang, Y., Wu, Q., Hu, Z., Han, X., Xu, Y., Deng, H. and Pan, J. (2014). FLA8/KIF3B phosphorylation regulates kinesin-II interaction with IFT-B to control IFT entry and turnaround. *Dev. Cell* **30**, 585-597.

Loktev, A. V., Zhang, Q., Beck, J. S., Searby, C. C., Scheetz, T. E., Bazan, J. F., Slusarski, D. C., Sheffield, V. C., Jackson, P. K. and Nachury, M. V. (2008). A BBSome subunit links ciliogenesis, microtubule stability, and acetylation. *Dev. Cell* **15**, 854-865.

Ludington, W. B., Wemmer, K. A., Lechtreck, K. F., Witman, G. B. and Marshall, W. F. (2013). Avalanche-like behavior in ciliary import. *Proc. Natl. Acad. Sci. USA* **110**, 3925-3930.

Luo, M., Cao, M., Kan, Y., Li, G., Snell, W. and Pan, J. (2011). The phosphorylation state of an aurora-like kinase marks the length of growing flagella in *Chlamydomonas*. *Curr. Biol.* **21**, 586-591.

Madhivanan, K. and Aguilar, R. C. (2014). Ciliopathies: the trafficking connection. *Traffic* **15**, 1031-1056.

Marshall, W. F. and Rosenbaum, J. L. (2001). Intraflagellar transport balances continuous turnover of outer doublet microtubules: implications for flagellar length control. *J. Cell Biol.* **155**, 405-414.

Marshall, W. F., Qin, H., Rodrigo Brenni, M. and Rosenbaum, J. L. (2005). Flagellar length control system: testing a simple model based on intraflagellar transport and turnover. *Mol. Biol. Cell* **16**, 270-278.
Mencarelli, C., Mitchell, A., Leoncini, R., Rosenbaum, J. and Lupetti, P. (2013). Isolation of intraflagellar transport trains. *Cytoskeleton* **70**, 439-452.
Mukhopadhyay, S., Wen, X., Chih, B., Nelson, C. D., Lane, W. S., Scales, S. J. and Jackson, P. K. (2010). TULP3 bridges the IFT-A complex and membrane phosphoinositides to promote trafficking of G protein-coupled receptors into primary cilia. *Genes Dev.* **24**, 2180-2193.
Nachury, M. V., Loktev, A. V., Zhang, Q., Westlake, J., Peränen, J., Merdes, A., Slusarski, D. C., Sheller, R. H., Bazan, J. F., Sheffield, V. C. et al. (2007). A core complex of BBS proteins cooperates with the GTPase Rab8 to promote ciliary membrane biogenesis. *Cell* **129**, 1201-1213.
Ou, G., Blacque, O. E., Snow, J. J., Leroux, M. R. and Scholey, J. M. (2005). Functional coordination of intraflagellar transport motors. *Nature* **436**, 583-587.
Pan, J., Wang, Q. and Snell, W. J. (2004). An aurora kinase is essential for flagellar disassembly in Chlamydomonas. *Dev. Cell* **6**, 445-451.
Pan, J., Seeger-Nukpezah, T. and Golemis, E. A. (2013). The role of the cilium in normal and abnormal cell cycles: emphasis on renal cystic pathologies. *Cell. Mol. Life Sci.* **70**, 1849-1874.
Pazour, G. J., Wilkerson, C. G. and Witman, G. B. (1998). A dynein light chain is essential for the retrograde particle movement of intraflagellar transport (IFT). *J. Cell Biol.* **141**, 979-992.
Pazour, G. J., Dickert, B. L. and Witman, G. B. (1999). The DHC1b (DHC2) isoform of cytoplasmic dynein is required for flagellar assembly. *J. Cell Biol.* **144**, 473-481.
Pazour, G. J., Dickert, B. L., Vucica, Y., Seeley, E. S., Rosenbaum, J. L., Witman, G. B. and Cole, D. G. (2000). *Chlamydomonas IFT*88 and its mouse homologue, polycystic kidney disease gene Tg737, are required for assembly of cilia and flagella. *J. Cell Biol.* **151**, 709-718.
Pedersen, L. B., Geimer, S. and Rosenbaum, J. L. (2006). Dissecting the molecular mechanisms of intraflagellar transport in *Chlamydomonas*. *Curr. Biol.* **16**, 450-459.
Pigino, G., Geimer, S., Lanzavecchia, S., Paccagnini, E., Cantele, F., Diener, D. R. Rosenbaum, J. L. and Lupetti, P. (2009). Electron-tomographic analysis of intraflagellar transport particle trains in situ. *J. Cell Biol.* **187**, 135-148.
Porter, M. E., Bower, R., Knott, J. A., Byrd, P. and Dentler, W. (1999). Cytoplasmic dynein heavy chain 1b is required for flagellar assembly in Chlamydomonas. *Mol. Biol. Cell* **10**, 693-712.
Qin, H., Diener, D. R., Geimer, S., Cole, D. G. and Rosenbaum, J. L. (2004). Intraflagellar transport (IFT) cargo: IFT transports flagellar precursors to the tip and turnover products to the cell body. *J. Cell Biol.* **164**, 255-266.
Qin, H., Burnette, D. T., Bae, Y.-K., Forscher, P., Barr, M. M. and Rosenbaum, J. L. (2005). Intraflagellar transport is required for the vectorial movement of TRPV channels in the ciliary membrane. *Curr. Biol.* **15**, 1695-1699.
Rampolas, P., Pedersen, L. B., Patel-King, R. S. and King, S. K. (2007). Chlamydomonas FAP133 is a dynein intermediate chain associated with the retrograde intraflagellar transport motor. *J. Cell Sci.* **120**, 3653-3665.
Reynolds, E. S. (1963). The use of lead citrate at high pH as an electron-opaque stain in electron microscopy. *J. Cell Biol.* **17**, 208-212.
Rosenbaum, J. L. and Child, F. M. (1967). Flagellar regeneration in protozoan flagellates. *J. Cell Biol.* **34**, 345-364.
Rosenbaum, J. L., Moulder, J. E. and Ringo, D. L. (1969). Flagellar elongation and shortening in Chlamydomonas: the use of cycloheximide and colchicine to study the synthesis and assembly of flagellar proteins. *J. Cell Biol.* **41**, 600-619.
Sager, R. and Granick, S. (1953). Nutritional studies with *Chlamydomonas reinhardii*. *Ann. N. Y. Acad. Sci.* **56**, 831-838.
Salvi, E., Cantele, F., Zampighi, L., Fain, N., Pigino, G., Zampighi, G. and Lanzavecchia, S. (2008). JUST (Java User Segmentation Tool) for semi-automatic segmentation of tomographic maps. *J. Struct. Biol.* **161**, 287-297.
Seo, S., Guo, D.-F., Bugge, K., Morgan, D. A., Rahmouni, K. and Sheffield, V. C. (2009). Requirement of Bardet-Biedl syndrome proteins for leptin receptor signaling. *Hum. Mol. Genet.* **18**, 1323-1331.
Silva, D. A., Huang, X., Behal, R. H., Cole, D. G. and Qin, H. (2012). The RABL5 homolog IFT22 regulates the cellular pool size and the amount of IFT particles partitioned to the flagellar compartment in Chlamydomonas reinhardtii. *Cytoskeleton* **69**, 33-48.
Snow, J. J., Ou, G., Gunnarson, A. L., Walker, M. R., Zhou, H. M., Brust-Mascher, I. and Scholey, J. M. (2004). Two anterograde intraflagellar transport motors cooperate to build sensory cilia on C. elegans neurons. *Nat. Cell Biol.* **6**, 1109-1113.
Su, X., Driscoll, K., Yao, G., Raed, A., Wu, M., Beales, P. L. and Zhou, J. (2014). Bardet-Biedl syndrome proteins 1 and 3 regulate the ciliary trafficking of polycystic kidney disease 1 protein. *Hum. Mol. Genet.* **23**, 5441-5451.
Suryavanshi, S., Eddé, B., Fox, L. A., Guerrero, S., Hard, R., Hennessey, T., Kabi, A., Malison, D., Pennock, D., Sale, W. S. et al. (2010). Tubulin glutamylation regulates ciliary motility by altering inner dynein arm activity. *Curr. Biol.* **20**, 435-440.
Taschner, M., Bhogaraju, S., Vetter, M., Morawetz, M. and Lorentzen, E. (2011). Biochemical mapping of interactions within the intraflagellar transport (IFT) B core complex: IFT52 binds directly to four other IFT-B subunits. *J. Biol. Chem.* **286**, 26344-26352.
Taschner, M., Kotsis, F., Brauer, P., Kuehn, E.W. and Lorentzen, E. (2014). Crystal structures of IFT70/52 and IFT52/46 provide insight into intraflagellar transport B core complex asembly. *J. Cell Biol.* **207**, 269-282.
Taschner, M., Bhogaraju, S. and Lorentzen, E. (2012). Architecture and function of IFT complex proteins in ciliogenesis. *Differentiation* **83**, S12-S22.
Thoma, C. R., Frew, I. J., Hoerner, C. R., Montani, M., Moch, H. and Krek, W. (2007). pVHL and GSK3beta are components of a primary cilium-maintenance signalling network. *Nat. Cell Biol.* **9**, 588-595.
Torisawa, T., Ichikawa, M., Furuta, A., Saito, K., Oiwa, K., Kojima, H., Toyoshima, Y. Y. and Furuta, K. (2014). Autoinhibition and cooperative activation mechanisms of cytoplasmic dynein. *Nat. Cell Biol.* **16**, 1118-1124.
Tsao, C.-C. and Gorovsky, M. A. (2008). Different effects of Tetrahymena IFT172 domains on anterograde and retrograde intraflagellar transport. *Mol. Cell. Biol.* **19**, 1450-1461.
van Heel, M. and Schatz, M. (2005). Fourier shell correlation threshold criteria. *J. Struct. Biol.* **151**, 250-262.
Vashishtha, M., Walther, Z. and Hall, J. L. (1996). The kinesin-homologous protein encoded by the Chlamydomonas FLA10 gene is associated with basal bodies and centrioles. *J. Cell Sci.* **109**, 541-549.
Viswanadha, R., Hunter, E. L., Yamamoto, R., Wirschell, M., Alford, L. M., Dutcher, S. K. and Sale, W. S. (2014). The ciliary inner dynein arm, I1 dynein, is assembled in the cytoplasm and transported by IFT before axonemal docking. *Cytoskeleton* **71**, 573-586.
Walther, Z., Vashishtha, M. and Hall, J. L. (1994). The Chlamydomonas FLA10 gene encodes a novel kinesin-homologous protein. *J. Cell Biol.* **126**, 175-188.
Wei, Q., Zhang, Y., Li, Y., Zhang, Q., Ling, K. and Hu, J. (2012). The BBSome controls IFT assembly and turnaround in cilia. *Nat. Cell Biol.* **14**, 950-957.
Wei, Q., Xu, Q., Zhang, Y., Li, Y., Zhang, Q., Hu, Z., Harris, P. C., Torres, V. E., Ling, K. and Hu, J. (2013). Transition fibre protein FBF1 is required for the ciliary entry of assembled intraflagellar transport complexes. *Nat. Commun.* **4**, 2750.
Wilson, N. F. and Lefebvre, P. A. (2004). Regulation of flagellar assembly by glycogen synthase kinase 3 in Chlamydomonas reinhardtii. *Eukaryot. Cell* **3**, 1307-1319.
Wood, C. R. and Rosenbaum, J. L. (2014). Proteins of the ciliary axoneme are found on cytoplasmic membrane vesicles during growth of cilia. *Curr. Biol.* **24**, 1114-1120.
Wren, K. N., Craft, J. M., Tritschler, D., Schauer, A., Patel, D. K., Smith, E. F., Porter, M., Kner, P. and Lechtreck, K. F. (2013). A differential cargo-loading model of ciliary length regulation by IFT. *Curr. Biol.* **23**, 2463-2471.